

Accepted Manuscript

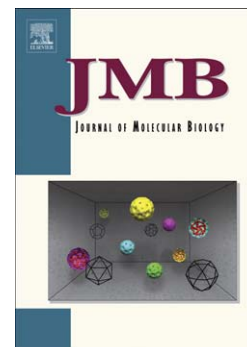
Specific recognition of a DNA immunogen by its elicited antibody

Santiago Sanguinetti, Juan M. Centeno Crowley, María F. Lodeiro Merlo, María L. Cerutti, Ian A. Wilson, Fernando A. Goldbaum, Robyn Stanfield, Gonzalo de Prat-Gay

PII: S0022-2836(07)00538-4
DOI: doi: [10.1016/j.jmb.2007.04.046](https://doi.org/10.1016/j.jmb.2007.04.046)
Reference: YJMBI 59353

To appear in: *Journal of Molecular Biology*

Received date: 19 January 2007
Revised date: 10 April 2007
Accepted date: 18 April 2007



Please cite this article as: Sanguinetti, S., Crowley, J.M.C., Merlo, M.F.L., Cerutti, M.L., Wilson, I.A., Goldbaum, F.A., Stanfield, R. & de Prat-Gay, G., Specific recognition of a DNA immunogen by its elicited antibody, *Journal of Molecular Biology* (2007), doi: [10.1016/j.jmb.2007.04.046](https://doi.org/10.1016/j.jmb.2007.04.046)

This is a PDF file of an unedited manuscript that has been accepted for publication. As a service to our customers we are providing this early version of the manuscript. The manuscript will undergo copyediting, typesetting, and review of the resulting proof before it is published in its final form. Please note that during the production process errors may be discovered which could affect the content, and all legal disclaimers that apply to the journal pertain.

Specific Recognition of a DNA Immunogen by its Elicited Antibody

Santiago Sanguineti¹, Juan M. Centeno Crowley¹, María F. Lodeiro Merlo¹, María L. Cerutti¹, Ian A. Wilson², Fernando A. Goldbaum¹, Robyn Stanfield²¶, & Gonzalo de Prat-Gay¹¶

¹ Instituto Leloir and CONICET, Patricias Argentinas 435, 1405 Buenos Aires, Argentina
and ²Dept. of Molecular Biology and the Skaggs Institute for Chemical Biology, The Scripps
Research Institute, 10550 N. Torrey Pines Road, La Jolla, CA 92037, USA.

Running title: DNA recognition by its elicited antibody

Keyword: Anti-DNA; Structure; Antibody; autoimmune; DNA binding

¶ Corresponding authors gpratgay@leloir.org.ar; robyn@scripps.edu

SUMMARY

DNA recognition by antibodies is a key feature of autoimmune diseases yet model systems with structural information are very limited. The monoclonal antibody ED-10 recognizes one of the strands of the DNA duplex used in the immunogenic complex. Modifications of the 5' end decrease the binding affinity and short oligonucleotides retain high binding affinity. We determined crystal structures for the Fab bound to a 6mer oligonucleotide containing the specific sequence that raised the antibody and compared it with the unliganded Fab. Only the first two bases from the 5' end (dTdC) display electron density and we observe 4 key hydrogen bonds at the interface. The thymine ring is stacked between TrpH50 and TrpH95, and the cytosine ring is packed against TyrL32. Upon DNA binding, TyrH97 and TrpH95 rearrange to allow subnanomolar binding affinity, five orders of magnitude higher than other complexes, possibly because of having gone through affinity maturation in this, the first antibody-DNA immunogen complex described in atomic detail.

INTRODUCTION

Nucleic acid recognition by proteins is required for essential gene related functions such as DNA replication, transcription, repair and recombination, or splicing and protein synthesis in the case of RNA. A wide number of recognition strategies involving different conformations, interfaces and thermodynamics are evident from the large number of protein-nucleic acid systems that have been characterized, with 1560 protein-nucleic acid complex structures deposited in the PDB to date ¹. A wealth of information is now available on how antibodies recognize proteins in terms of structure, thermodynamics and kinetics ^{2; 3}. In contrast, and despite its relevance, there is little information about structure and mechanism of DNA recognition, in part because of the low antigenicity of DNA and the difficulties in raising antibodies against it ⁴.

Antibodies can react with DNA even though DNA is known to be a poor immunogen *per se*. Anti-DNA antibodies are found in patients with Systemic Lupus Erythematosus (SLE) and related autoimmune diseases. These diseases are characterized by the spontaneous production of auto-antibodies directed towards a variety of nuclear antigens such as histones and DNA ^{5; 6 7; 8; 9; 10; 11; 12; 13; 14; 15}. With no specificity for particular DNA sequences ^{16; 17; 18}, most anti-DNA auto-antibodies are classified based on their ability to recognize single or double stranded DNA ^{19; 20; 21}.

Although anti-DNA antibodies represent a special class of DNA-binding proteins, only a handful of structures of nucleic acid bound antibodies have been determined to date ^{20; 21; 22; 23; 24}. The first structures reported were for the unliganded and d(pT)₃ bound forms of the murine anti-DNA antibody BV04-01 ²⁰. Besides providing a first glimpse of Fab-DNA binding interactions, these two structures provided the first examples of conformational change between the free and ligand-bound antibodies. The determination of the structure of the DNA-1 anti-DNA Fab bound to dT₅ ²⁵ led to the proposal of a ssDNA recognition motif termed the “ssDNA-antibody recognition module” or “D-ARM” (see discussion) ²⁵. These results were recently complemented with the determination of the structure of the DNA-1 Fab, unbound and with dT₃ ²⁶. Thermodynamic characterization of the DNA-1/DNA interactions have been carried out for non-specific poly-dT ligands, which showed very low affinity ^{27; 28}.

DNA binding studies with anti-DNA antibodies have been carried out in many different systems ^{29; 30; 31}. However, in terms of a detailed mechanistic analysis, the best described is that of the 11F8 anti-ssDNA monoclonal Fab ^{32; 33}. All the systems described so far correspond to natural autoantibodies obtained from mice where no information of the immunogen (DNA or other) is available, and the ssDNA ligands must therefore be selected arbitrarily. In the case of the antibody 11F8, the ssDNA ligands were isolated by PCR selection methods for high affinity binding (SELEX)

Using the 18mer DNA binding site 35 of the human papillomavirus (HPV) strain 16 E2 protein (E2c) bound to the protein as immunogen, we have obtained anti-DNA monoclonal antibodies (mAbs) that bind DNA duplexes containing the binding site of HPV E2C with sub-nanomolar dissociation constants. The discrimination factors (K_D specific/ K_D non-specific) range from 125- to 20000-fold, where the most extensively described antibody to date is ED-10³⁴. Further analysis demonstrated the absence of electrostatic interactions stabilizing the complex, and an unusual positive heat capacity change that suggested a substantial rearrangement in the DNA fragments with possible contribution from conformational changes in the antibody combining site. This conformational change is supported by a reaction rate 4 orders of magnitude slower than that of the natural protein ($1.5 \times 10^9 \text{ M}^{-1} \text{ s}^{-1}$), indicating a higher energetic barrier for the binding reaction, and assignable to a substantial conformational change and the lack of an electrostatic component³⁵.

In the present work, we show that the anti-DNA ED-10 mAb can recognize the 5'-end of the 18mer site 35-18 strand B E2 binding site, in the context of single or double-stranded DNA, with higher affinity for single than for the double-stranded DNA. We have crystallized the ED-10 Fab unliganded, and with a 6-mer single-stranded oligonucleotide corresponding to the 5' end of site 35-18 strand B. The structures of the free and DNA-bound ED-10 reveal that the antibody binds ssDNA by stacking the bases between aromatic residues in the CDRs, and uses the D-ARM motif described previously for DNA-1, BV04-01, and Jel 103²⁵. These results represent the first structural and thermodynamic study of an antibody/DNA complex comprised of the DNA antigen and its corresponding elicited antibody.

RESULTS

DNA Binding

Our initial characterization of the ED-10 antibody showed that it was able to tightly bind a series of DNA duplexes that contained the sequence of 18 base pairs used as immunogen: site 35-18ds (Figure 1A)³⁴. DNase protection experiments systematically failed to identify a significant stretch of consecutive bases around the E2 DNA site 35 involved in the binding (not shown). We had previously observed that phosphorylation of the 5' OH of chain B led to a decrease in the affinity, which added evidence to the possibility that ED-10 recognizes the 5' end of this chain³⁴. Considering the evidence mentioned above, we decided to analyze the binding of ED-10 to chain B. To our surprise, the antibody binds to this ssDNA with an equilibrium dissociation constant (K_D) of 0.4 nM, a four-fold higher affinity than for the double stranded 35-18 reference duplex (Figure 1B and Table I). The site 35-18 is quasi-palindromic and the expected hairpins formed by each single stranded chain are similar, yet still there is a 6,000-fold difference in the binding affinity compared to site 35-18 strand A, corresponding to 5.0 kcal mol⁻¹ of binding free energy change. These results suggest that it is the end sequence at the 5' end of chain B that contains the main antibody binding determinant.

Binding experiments using a DNA duplex of 48 base pairs containing site 35-18 at the centre but bearing a different sequence at the 5' end of chain B (site35-48ds) showed a ~250-fold drop in the K_D compared with 35-18ds (Table I). On the other hand, ED-10 binds a similar size duplex with a random sequence (iset 35-48ds) with the same dissociation constant as to site 35-48ds (Figure 1A, Table I). Since these results further support the recognition of the 5' end of chain B from site 35-18, we designed shorter versions of this oligonucleotide that conserved the 5' sequence. The binding affinity remains virtually the same irrespective of the oligonucleotide length as long as the sequence 5'-TC is present (average K_D 0.2 nM, ΔG 13.0 kcal mol⁻¹) (Figure 1A, Table I). Finally, if we mutate the 5'-T to any other base in the 18mer site 35, the affinity drops dramatically ($\Delta\Delta G$ ~5.0 kcal mol⁻¹) (Table I).

Our previous results had shown that the duplex DNAs underwent a conformational change or partial melting of structure upon binding of the antibody³⁵, which made us wonder whether the antibody had the ability to separate the strands and bind chain B. An electrophoresis mobility shift assay (EMSA) experiment with site 35-18 duplex shows that the bound, shifted DNA remains double stranded (Figure 1C, left panel), with no evidence of ssDNA oligonucleotide detectable. In addition, a similar experiment confirmed the spectroscopic binding results for chain A of single stranded site 35 DNA 18mer (Figure 1C, middle panel), and for the 80 mer (Figure 1C, right panel). This later result, together with previous binding data for a 166 mer fragment³⁵ show that the antibody can bind long stretches of DNA by its 5'-TC end.

Crystal Structures of free and DNA bound ED10 Fabs

The ED-10 Fab fragment was crystallized in its free form and in the presence of a single-stranded 6-mer (5'-TCA ACC-3'). Both structures were determined by the molecular replacement (MR) method to resolutions of 2.73Å (free) and 1.89Å (DNA bound) with R/R_{free} values of 20.1%/26.4% (free) and 17.7%/20.4% (DNA bound) and good stereochemistry (Figure 2A, Table 2). There are two Fab fragments in the asymmetric unit of the free structure with elbow angles of 174° and 173°, and one Fab-DNA complex in the asymmetric unit of the DNA-bound Fab of 184°. There is clear electron density for only the first two bases on the 5' end of the DNA used for co-crystallization (5'-TC-3') (Figure 2B). The antibody complementarity determining region (CDR) loops belong to the canonical classes predicted from their sequences: L1, class 4; L2, class 1; L3 class 1; H1 class 1^{36, 37} (Fab light and heavy chains are denoted by L and H chain identifiers) except for H2, which is unusually short and represents a new canonical class. Currently, there are 4 canonical classes defined for H2 CDR loops, with class 1 having no inserts after residue 52, class 2 and 3 having one insert after residue 52, and class 4 with three inserts after residue 52. The H2 CDR loop in ED-10 has a deletion at residue 53, making it one residue shorter than the loops in canonical class 1 (Figure 3).

The DNA binding site

Electron density is very clear and well-ordered for two nucleotides, dTdC in the Fab binding site (Figure 2B). Both nucleotides adopt *anti* conformations, with torsion angles about their N-glycosidic bonds of -133° (Thy¹) and -107° (Cyt²). Both sugars are in the C2' endo conformation with pseudorotation phase angles (P) of 162° (Thy¹) and 158° (Cyt²). The DNA binds with the two bases buried in the Fab combining site, and the phosphate group on the surface (Figure 4). The DNA makes four hydrogen bonds to Fab (Figure 4, Table 3) residues in CDRs L1, L3, H1 and H3 and four hydrogen bonds to waters. There is also an NH-aromatic hydrogen bond³⁸ between Thy¹ N3 and Tyr^{H33}, with a distance between the center of the Tyr ring and the N3 of 3.4Å. The Thy¹ base is stacked between Trp^{H50} and Trp^{H95}, while Cyt² is stacked against Tyr^{L32} and roughly perpendicular to Trp^{H95}. The molecular surface area buried on the Fab is 385Å², while 306Å² is buried on the dinucleotide, 55% and 45% from Thy¹ and Cyt², respectively. A total of 184 van der Waals' contacts are made between the Fab and dTdC and the shape correlation statistic (S_c) is 0.73³⁹.

Futher binding studies

Given the structure found at the combining site, where only electron density for the 5'-TC end of the hexanucleotide was observed, we tested oligonucleotides of smaller sizes. The dissociation constants for 5'-TCA, 5'-TC, were 0.3 ± 0.01 nM and 0.2 ± 0.02 nM, respectively, identical to the tetranucleotide (Table 1). The mononucleotide phosphate, dTTP binds very weakly ($K_D \geq 0.5$ μ M, not shown), but the mononucleoside analog, dThymidine (lacking the phosphate group), displays a K_D of 2.7 ± 0.5 nM, suggesting that the phosphate groups in the dTTP are involved in repulsive interactions or are sterically hindered. The difference in binding energy between the single dT and the 5'-TC is 1.0 kcal mol⁻¹. Since the dissociation constants of higher affinity are close to the limit of detection we estimate that this difference in binding energy is at least 10% of the overall binding energy (13 kcal mol⁻¹). There appears to be little if any contribution from bases 3 and beyond, and no electron density was observed in the crystals. However, we cannot discriminate at this stage whether this is due to mobility or to DNA cleavage because of the long incubation periods in the crystallization cocktails.

Conformational change of the antibody

Conformational changes can be observed between the Fab combining sites of the free and DNA-bound ED-10. When the heavy and light variable domains (V_H and V_L) from the free (two Fabs in the asymmetric unit) and DNA-bound (one Fab in the asymmetric unit) structures are superimposed using non-CDR residues, the root mean square deviations (\AA) for the CDR $C\alpha$ coordinates are L1 (1.01, 0.96), L2 (0.41, 0.38), L3 (0.49, 0.49), H1 (0.31, 0.31), H2 (0.65, 0.61), and H3 (1.49, 1.49). The largest change in CDR H3, is centered around residues H96-H98 with a 3.8\AA change in $C\alpha$ position of residue Tyr^{H97}, which is at the tip of CDR H3 that moves away from the center of the antibody combining site to allow DNA binding (Figure 5A, B). The CDR L1 loop is long, with a five amino-acid insert after residue L27. The largest movement of this loop is centered around the residues at the tip (L28-29) and this loop also moves away from the center of the binding site to allow DNA binding.

In order to determine the presence of a conformational change upon binding of the DNA immunogen in solution, we carried out circular dichroism experiments. The far-UV circular dichroism of the Fab displays the expected β -sheet dominance with a minimum at 216 nm (Figure 6A) and a maximum at 233 nm. The single stranded 5'-TCAA oligonucleotide shows a small contribution in that region compared to that of the protein. The spectra of the complex shows a substantial difference with respect to the sum of the individual spectra, in particular a decrease in the negative band at 216 nm and a noticeable disappearance of a band at around 230 nm. This band was originally assigned in an immunoglobulin to the contribution of aromatic side chains to the spectra, and also suggested in other proteins^{40; 41; 42}. In principle, the change at 216 nm is

normally considered to report changes in β -sheet content, however, comparison of different Fabs produced even larger changes in that band, where the β -sheet content cannot be expected to be modified to such an extent, and was also assigned to the contributions of aromatic side chains⁴¹;
⁴²

The near UV-CD of the protein displays a typical but small band between 280 and 290 nm, expected for the contribution of aromatic side chains in an asymmetric environment (Figure 6B). The oligonucleotide also shows a weak and broad band around the same region, but the complex shows a large and distinctive positive band at 268 nm, not observed at all in the isolated ligand (Figure 6B). With the structural information of the binding site at hand, we can assign this change to the stacking between the base rings of the oligonucleotide and the aromatic side chains of the antibody. Thus, the near-UV is very sensitive to base-aromatic side chain stacking interaction, at least comparable to the known base-base stacking in nucleic acids⁴².

DISCUSSION

Understanding the structural and thermodynamic basis for DNA recognition by antibodies is highly relevant for two fundamental aspects in biology. The first is how DNA, a “self” molecule, is recognized by the immune system. Our understanding of this recognition mechanism lags far behind that of the immune recognition of proteins and other biomolecules. The second major aspect is that the anti-DNA immune response lies behind a group of severe autoimmune diseases of which the most representative is SLE. In order to better understand these problems, we need to utilize a combination of mechanistic and structural approaches in relevant systems, where if possible the antibody comes from the immune response elicited by the ligand used as immunogen.

The need for more crystal structures of anti-DNA antibodies arise from the fact that, despite numerous molecular modeling studies of anti-DNA combining sites can be found in the literature^{43; 44}, the scarcely available crystal structures of antibody-DNA complexes indicate that DNA causes significant conformational changes in the antibody when bound (^{20; 26} and this work). In addition, the exact docking of the ligands may not be precisely modeled as additional interactions will arise from both the antibody variability and the different base ligands. Therefore, it is difficult to obtain reliable, high resolution, models without crystallographic data, even though homology modeling of antibody hypervariable loops is a widely used technique. An example of this is the remarkably high difference in binding affinity between ED10 and DNA1 for their respective ligands, something not possibly anticipated based on the structures (see below).

The structure of the ED-10-oligonucleotide complex is only the third antibody-DNA structure to be determined to date. Previous work comparing the nucleotide binding sites of DNA-1²⁵ with those of BV04-01²⁰ and Jel 103²², has suggested that antibodies make use of a conserved binding motif for recognizing single-stranded DNA. This motif was termed the D-ARM²⁵ and has been located in the DNA-1, BV04-01 and Jel 103 binding sites. The ED-10 binding site described here also displays the D-ARM motif (Figure 7). In ED-10, Cyt² binds into the D-ARM, with the Cyt² ring stacked against the Tyr^{L32} ring and roughly perpendicular to the Trp^{H95} ring system in the tip of CDR H3. Cyt² then makes hydrogen bond to L91, although in ED-10, binds to the main chain carbonyl from of Gly^{L91}, rather than to the side-chain and accepts a hydrogen bond from the main chain amide from Gly^{H98}. Thus, to the original description of the D-ARM as having a hydrogen bonding residue at L91, we can extend the definition to include any hydrogen bonding atom. Residue L32 is a Tyrosine in 71% of κ and 50% of λ chains surveyed in the 2000 version of the Kabat database⁴⁵, while residue H95 is far more variable.

The binding affinity of the ED-10/5'-TC is 0.35 nM, compared to 27 μ M for the DNA-1/dT5 complex^{28; 46}. This 80,000-fold difference clearly shows how the ED-10 antibody selected after immunization with the E2c/Site 35-18³⁴ was optimized for high affinity, with a binding free energy

difference of 6.7 kcal mol⁻¹ with respect to the DNA-1/dT5 complex, where dT5 was not the immunogen that gave rise to that antibody. It is difficult to reconcile such large differences in binding affinity with the structural results, as both complexes bury similar size surface areas (385Å²/306Å² for ED-10 (Fab/DNA) and 402Å²/404Å² for DNA1, and each has four hydrogen bonds from Fab to DNA. Indeed, the DNA-1 complex has a more complementary interface, with an S_c value of 0.82 versus 0.73 for the ED-10 complex. Moreover, while the affinity of DNA-1 for long dT ligands increases from 27 to 0.15 μM for dT15⁴⁶, the affinity of ED-10 for 80mers remains sub-nanomolar (this work). Thus, it would be interesting to know whether the long dT ligands make additional contacts with the DNA-1 CDRs or whether the secondary or tertiary structure of the oligonucleotide affects binding. Clearly, inspection of the structures simply cannot anticipate the strength of the different bonds that make up the binding interface and the thermodynamic measurements provide the final answer. However, we must keep in mind that the ED10-DNA interaction went through the process of antigen maturation as it is the result of an actual immunization, and this is the most likely basis for such a large difference in binding affinity, approaching five orders of magnitude^{28; 34; 46}.

Conformational changes between free and bound Fabs have been reviewed extensively⁴⁷:⁴⁸. Changes range from side-chain movement to movement of CDR loops as more or less rigid bodies, to total rearrangement of CDR loop conformation (and combinations of the above). While CDR H3 is most often involved in any conformational change, other CDR loops can also be involved. In addition, the V_L and V_H domains can move relative to one another to help recreate a binding site suitable for antigen binding. Conformational changes between the free and bound Fabs have been seen for both the BV04-01 and DNA-1 systems, however this is probably not because of their DNA-binding activities, but just because conformational changes in free versus bound Fabs are so common. The changes we can observe in the ED-10 CDRs L1 and H3 maintain the overall CDR conformation, with the CDRs moving as rigid bodies away from the center of the binding site. In summary, we can explain the unusually high affinity of ED10 towards dTdC by an induced fit mechanism that allows for an extensive and tight stacking of both bases between aromatic side chains, maximizing the number of contacts and burying the nucleic acid on a deep pocket at the center of the combining site, that was formed precisely as a consequence of the binding event and the associated conformational change.

As a complement of crystallographic studies, we investigated the binding-associated conformational changes by spectroscopic methods in solution. Both far and near -UV regions of the CD spectra are dominated by aromatic contributions from side chains. The large change in the near UV is indicative of stacking of the dTdC bases between the aromatics, in excellent agreement with the interactions observed in the crystal structure. In any case, these contributions do not allow

to discriminate or assign secondary structure changes in the antibody by this method, such as that observed in the structure of the complex. Interestingly, the stacking of base rings against aromatic side chains gives a change in ellipticity as large or larger than that observed for the stacking of bases in nucleic acids.

In summary, we determined the energetic contribution of bases and the structure of anti-DNA antibody/DNA immunogen complex, which presents a similar recognition module to a natural autoimmune antibody, and a substantial conformational change. The main determinant for the binding affinity by the monoclonal antibody ED-10 is located in the first two bases of the 5'end of one DNA chain, irrespective of the length or whether it is double or single stranded DNA, suggesting possible uses as a molecular biology tool or possible diagnostic applications. Nevertheless, in addition to the understanding of the molecular basis of DNA recognition in autoimmune disease, this work opens the door for the design of compounds that potentially bind pathogenic antibodies, with consequent therapeutic implications. Finally, the strategy by which the immune system responds to a "self" molecule such as DNA remains puzzling, and makes us wonder how the immunogen has to be processed and presented in order, as in this case, to recognize the 5'end of a DNA fragment.

MATERIALS AND METHODS

Proteins and DNAs.

ED-10 IgG was purified from ascites fluids and the derived Fab fragments prepared following standard procedures³⁴. Fabs were titrated weekly with DNA and were shown to retain the 100% binding activity for at least 2 months. Fab fragments of the antibodies were used for binding experiments throughout the work to simplify the binding analysis, unless stated otherwise.

The sequence of the B chain of the reference oligonucleotide is 5'-TCAACCGATTTCGGTTAC-3', corresponding to E2 site 35 in the HPV-16 genome. All DNA oligonucleotides were obtained from IDT (Coralville, IA, USA). Long oligonucleotides were purified by SDS-PAGE by the manufacturer and all were tested for duplex formation by native gel electrophoresis. The concentration of the single and double stranded DNA was calculated from extinction coefficients (Cantor, byopolymers).

Fluorescence binding experiments.

Tryptophan fluorescence titrations were carried out with excitation at 285 nm and the emission monitored at 340 nm, using an Aminco Bowman Series 2 spectrofluorimeter. The proteins were incubated in TBS (25 mM Tris, 150 mM NaCl, pH 7.0) at 5 - 100 nM protein concentration in 3.0 ml volumes at 25 ± 0.1 °C. Double or single stranded DNA oligonucleotides were gradually added and the tryptophan fluorescence measured after a 5-minute equilibration at each point. The maximum dilution was 10% and the fluorescence was corrected accordingly. The data were fitted to a binding model where both protein and DNA concentrations are considered⁴⁹. ΔF is the difference in the signal between the Fab-DNA complex and free Fab, [DNA] and [Fab] are the oligonucleotide and protein concentration respectively and K_D is the dissociation constant for the interaction. The data were corrected for dilution.

Electrophoretic Mobility Shift Assays.

The ED-10 Fab/DNA complexes were incubated in TBS at room temperature for 30 minutes. The samples were separated by electrophoresis on a 20% acrylamide native gel in 0.5X TBE, at a constant current of 7 mA. The bands were visualized by standard ethidium bromide staining.

Crystallization and X-ray Data Collection.

Crystals of ED-10 were grown at room temperature by vapor diffusion in hanging drops against a reservoir solution containing 0.2 M ammonium sulfate, 0.1 M sodium cacodylate pH 6.5 and 25% polyethylene glycol monomethyl ether 2000. Briefly, a mixture of 1 μ l of protein stock and 1 μ l of the precipitating agent were equilibrated against 300 μ l of the same precipitating agent. Protein

concentration in the drop was 10 mg/ml. Diffraction data were collected to 2.73Å resolution at the ESRF (European Synchrotron Radiation Facility, Grenoble, France), beamline ID14-1 at room temperature, and processed with Denzo/Scalepack⁵⁰. The complex of ED-10/Fab-DNA (6-mer oligonucleotide 5'-TCAACC-3') was concentrated to 10 mg/ml in 25mM Tris-HCl, 150 mM NaCl, pH 7. Crystallization was performed at room temperature using the Jena Bioscience screens (Jena, Germany) according to the hanging drop method. The best diffracting crystals were obtained with the JBScreen Classic 4 solution B1 containing 15% PEG 6000, 0.05 M KCl; 0.01 M MgCl₂. Data were collected at the Protein Crystallography Beamline D03B-MX1 at the Laboratório Nacional de Luz Síncrotron, Campinas, Brazil at room temperature. X-ray diffraction data were processed with Denzo/Scalepack⁵⁰ to 1.89Å resolution.

Model Building, Refinement, and Analysis.

The unliganded ED-10 structure was determined by molecular replacement with the program AMoRe⁵¹ using Fab 50.1 (pdb code 1ggi) as a model. Model building was carried out with Tom/Frodo⁵² and the structure was refined with CNS⁵³ and Refmac⁵⁴ without TLS and with NCS restraints. The ED-10-DNA complex was determined by molecular replacement with the program EPMR⁵⁵ using the unliganded ED-10 Fab structure as a model. Model building was carried out with Tom/Frodo and the structure was refined with CNS and Refmac with TLS.

Circular Dichroism Spectroscopy.

Far and Near-UV circular dichroism spectra of ED-10, site 35-4 B and the complex were recorded in a Jasco J-810 spectropolarimeter. The samples were incubated in 25 mM Tris-HCl, 150 mM NaCl (pH 7) and data were collected at 25 ± 0.1 °C with a scan rate of 100 nm min⁻¹ in a 0.1 cm path length cuvette. Ten scans were averaged, and the raw ellipticity is shown, since the protein and DNA concentration were identical in all the cases (5 µM).

ACKNOWLEDGEMENTS

We thank Pedro Alzari for X-ray data collection of ED10 Fab and Sebastian Klinke for X-ray data collection of the complex. SS holds a Doctoral fellowship from Conicet, GPG is a Career investigator from CONICET. This work was supported by a grant from ANPCyT, PICT2000 8959. We thank assistance from the Laboratório Nacional de Luz Síncrotron (LNLS) under the project number D03B-CPR-3097/04.

REFERENCES

1. Berman, H. M., Westbrook, J., Feng, Z., Gilliland, G., Bhat, T. N., Weissig, H., Shindyalov, I. N. & Bourne, P. E. (2000). The Protein Data Bank. *Nucleic Acids Res* **28**, 235-42.
2. Braden, B. C. & Poljak, R. J. (1995). Structural features of the reactions between antibodies and protein antigens. *Faseb J* **9**, 9-16.
3. Davies, D. R. & Cohen, G. H. (1996). Interactions of protein antigens with antibodies. *Proc Natl Acad Sci U S A* **93**, 7-12.
4. Stollar, B. D. (1986). Antibodies to DNA. *CRC Crit Rev Biochem* **20**, 1-36.
5. Tan, E. M. (1989). Antinuclear antibodies: diagnostic markers for autoimmune diseases and probes for cell biology. *Adv Immunol* **44**, 93-151.
6. Koffler, D., Schur, P. H. & Kunkel, H. G. (1967). Glomerular localization of DNA and antibodies to nuclear constituents. *Trans Assoc Am Physicians* **80**, 149-55.
7. Pisetsky, D. S. (1992). Anti-DNA antibodies in systemic lupus erythematosus. *Rheum Dis Clin North Am* **18**, 437-54.
8. Pisetsky, D. S., Grudier, J. P. & Gilkeson, G. S. (1990). A role for immunogenic DNA in the pathogenesis of systemic lupus erythematosus. *Arthritis Rheum* **33**, 153-9.
9. Ben-Chetrit, E., Eilat, D. & Ben-Sasson, S. A. (1988). Specific inhibition of the DNA-anti-DNA immune reaction by low molecular weight anionic compounds. *Immunology* **65**, 479-85.
10. Blatt, N. B., Bill, R. M. & Glick, G. D. (1998). Characterization of a unique anti-DNA hybridoma. *Hybridoma* **17**, 33-9.

11. Blatt, N. B. & Glick, G. D. (1999). Anti-DNA autoantibodies and systemic lupus erythematosus. *Pharmacol Ther* **83**, 125-39.
12. Isenberg, D. A., Ehrenstein, M. R., Longhurst, C. & Kalsi, J. K. (1994). The origin, sequence, structure, and consequences of developing anti-DNA antibodies. A human perspective. *Arthritis Rheum* **37**, 169-80.
13. Murakami, H., Lam, Z., Furie, B. C., Reinhold, V. N., Asano, T. & Furie, B. (1991). Sulfated glycolipids are the platelet autoantigens for human platelet-binding monoclonal anti-DNA autoantibodies. *J Biol Chem* **266**, 15414-9.
14. Swanson, P. C., Yung, R. L., Blatt, N. B., Eagan, M. A., Norris, J. M., Richardson, B. C., Johnson, K. J. & Glick, G. D. (1996). Ligand recognition by murine anti-DNA autoantibodies. II. Genetic analysis and pathogenicity. *J Clin Invest* **97**, 1748-60.
15. Waer, M. (1990). The role of anti-DNA antibodies in lupus nephritis. *Clin Rheumatol* **9**, 111-4.
16. Stollar, B. D. (1994). Molecular analysis of anti-DNA antibodies. *Faseb J* **8**, 337-42.
17. Jang, Y. J., Sanford, D., Chung, H. Y., Baek, S. Y. & Stollar, B. D. (1998). The structural basis for DNA binding by an anti-DNA autoantibody. *Mol Immunol* **35**, 1207-17.
18. Jang, Y. J. & Stollar, B. D. (2003). Anti-DNA antibodies: aspects of structure and pathogenicity. *Cell Mol Life Sci* **60**, 309-20.
19. Cygler, M., Boodhoo, A., Lee, J. S. & Anderson, W. F. (1987). Crystallization and structure determination of an autoimmune anti-poly(dT) immunoglobulin Fab fragment at 3.0 Å resolution. *J Biol Chem* **262**, 643-8.
20. Herron, J. N., He, X. M., Ballard, D. W., Blier, P. R., Pace, P. E., Bothwell, A. L., Voss, E. W., Jr. & Edmundson, A. B. (1991). An autoantibody to single-stranded

- DNA: comparison of the three-dimensional structures of the unliganded Fab and a deoxynucleotide-Fab complex. *Proteins* **11**, 159-75.
21. Mol, C. D., Muir, A. K., Cygler, M., Lee, J. S. & Anderson, W. F. (1994). Structure of an immunoglobulin Fab fragment specific for triple-stranded DNA. *J Biol Chem* **269**, 3615-22.
 22. Pokkuluri, P. R., Bouthillier, F., Li, Y., Kuderova, A., Lee, J. & Cygler, M. (1994). Preparation, characterization and crystallization of an antibody Fab fragment that recognizes RNA. Crystal structures of native Fab and three Fab-monomucleotide complexes. *J Mol Biol* **243**, 283-97.
 23. Yokoyama, H., Mizutani, R., Satow, Y., Komatsu, Y., Ohtsuka, E. & Nikaido, O. (1999). Crystal structures of the 64M-2 and 64M-3 antibody Fabs complexed with DNA (6-4) photoproducts. *Nucleic Acids Symp Ser*, 267-8.
 24. Yokoyama, H., Mizutani, R., Satow, Y., Komatsu, Y., Ohtsuka, E. & Nikaido, O. (2000). Crystal structure of the 64M-2 antibody Fab fragment in complex with a DNA dT(6-4)T photoproduct formed by ultraviolet radiation. *J Mol Biol* **299**, 711-23.
 25. Tanner, J. J., Komissarov, A. A. & Deutscher, S. L. (2001). Crystal structure of an antigen-binding fragment bound to single-stranded DNA. *J Mol Biol* **314**, 807-22.
 26. Schuermann, J. P., Prewitt, S. P., Davies, C., Deutscher, S. L. & Tanner, J. J. (2005). Evidence for structural plasticity of heavy chain complementarity-determining region 3 in antibody-ssDNA recognition. *J Mol Biol* **347**, 965-78.
 27. Komissarov, A. A. & Deutscher, S. L. (1999). Thermodynamics of Fab-ssDNA interactions: contribution of heavy chain complementarity determining region 3. *Biochemistry* **38**, 14631-7.
 28. Schuermann, J. P., Henzl, M. T., Deutscher, S. L. & Tanner, J. J. (2004). Structure of an anti-DNA fab complexed with a non-DNA ligand provides insights into cross-reactivity and molecular mimicry. *Proteins* **57**, 269-78.

29. Ballard, D. W., Lynn, S. P., Gardner, J. F. & Voss, E. W., Jr. (1984). Specificity and kinetics defining the interaction between a murine monoclonal autoantibody and DNA. *J Biol Chem* **259**, 3492-8.
30. Chen, Y. & Stollar, B. D. (1999). DNA binding by the VH domain of anti-Z-DNA antibody and its modulation by association of the VL domain. *J Immunol* **162**, 4663-70.
31. Swanson, P. C., Cooper, B. C. & Glick, G. D. (1994). High resolution epitope mapping of an anti-DNA autoantibody using model DNA ligands. *J Immunol* **152**, 2601-12.
32. Ackroyd, P. C., Cleary, J. & Glick, G. D. (2001). Thermodynamic basis for sequence-specific recognition of ssDNA by an autoantibody. *Biochemistry* **40**, 2911-22.
33. Beckingham, J. A. & Glick, G. D. (2001). Sequence specific recognition of ssDNA by a lupus autoantibody: kinetics and mechanism of binding. *Bioorg Med Chem* **9**, 2243-52.
34. Cerutti, M. L., Centeno, J. M., Goldbaum, F. A. & Prat-Gay, G. d. (2001). Generation of sequence-specific, high affinity anti-DNA antibodies. *J Biol Chem* **276**, 12769-73.
35. Di Pietro, S. M., Centeno, J. M., Cerutti, M. L., Lodeiro, M. F., Ferreiro, D. U., Alonso, L. G., Schwarz, F. P., Goldbaum, F. A. & Prat-Gay, G. d. (2003). Specific antibody-DNA interaction: a novel strategy for tight DNA recognition. *Biochemistry* **42**, 6218-27.
36. Al-Lazikani, B., Lesk, A. M. & Chothia, C. (1997). Standard conformations for the canonical structures of immunoglobulins. *J Mol Biol* **273**, 927-948.

37. Martin, A. C. & Thornton, J. M. (1996). Structural families in loops of homologous proteins: automatic classification, modelling and application to antibodies. *Journal of Molecular Biology* **263**, 800-815.
38. Levitt, M. & Perutz, M. F. (1988). Aromatic rings act as hydrogen bond acceptors. *J Mol Biol* **201**, 751-4.
39. Lawrence, M. C. & Colman, P. M. (1993). Shape complementarity at protein/protein interfaces. *J Mol Biol* **234**, 946-50.
40. Azuma, T., Hamaguchi, K. & Migita, S. (1972). Denaturation of Bence Jones proteins by guanidine hydrochloride. *J Biochem (Tokyo)* **72**, 1457-67.
41. Tetin, S. Y. & Linthicum, D. S. (1996). Circular dichroism spectroscopy of monoclonal antibodies that bind a superpotent guanidinium sweetener ligand. *Biochemistry* **35**, 1258-64.
42. Tetin, S. Y., Prendergast, F. G. & Venyaminov, S. Y. (2003). Accuracy of protein secondary structure determination from circular dichroism spectra based on immunoglobulin examples. *Anal Biochem* **321**, 183-7.
43. Radic, M. Z., Mackle, J., Erikson, J., Mol, C., Anderson, W. F. & Weigert, M. (1993). Residues that mediate DNA binding of autoimmune antibodies. *J Immunol* **150**, 4966-77.
44. Rodkey, L. S., Gololobov, G., Rumbley, C. A., Rumbley, J., Schourov, D. V., Makarevich, O. I., Gabibov, A. G. & Voss, E. W., Jr. (2000). DNA hydrolysis by monoclonal autoantibody BV 04-01. *Appl Biochem Biotechnol* **83**, 95-103; discussion 103-5, 145-53.
45. Kabat, E. A., Wu, T. T., Perry, H. M., Gottesman, K. S. & Foeller, C. (1991). *Sequences of proteins of immunological interest*. 5 edit, 1, U.S. Department of health and human services.

46. Komissarov, A. A., Calcutt, M. J., Marchbank, M. T., Peletskaya, E. N. & Deutscher, S. L. (1996). Equilibrium binding studies of recombinant anti-single-stranded DNA Fab. Role of heavy chain complementarity-determining regions. *J Biol Chem* **271**, 12241-6.
47. Stanfield, R. L. & Wilson, I. A. (1994). Antigen-induced conformational changes in antibodies: a problem for structural prediction and design. *Trends Biotechnol* **12**, 275-9.
48. Stanfield, R. L. & Wilson, I. A. (2003). Antibody-antigen recognition and conformational changes. In *Handbook of Cell Signaling* (Bradshaw, R. & Dennis, E., eds.), Vol. 1, pp. 33-38. Elsevier Science, San Diego.
49. de Prat Gay, G. & Fersht, A. R. (1994). Generation of a family of protein fragments for structure-folding studies. 1. Folding complementation of two fragments of chymotrypsin inhibitor-2 formed by cleavage at its unique methionine residue. *Biochemistry* **33**, 7957-63.
50. Otwinowski, Z. & Minor, W. (1997). Processing of X-ray diffraction data collected in oscillation mode. *Meth. Enzymol.* **276A**, 307-326.
51. Navaza, J. (1994). AMoRe: an automated package for molecular replacement. *Acta Crystallogr.* **A50**, 157-163.
52. Jones, T. A. (1982). FRODO: a graphics fitting program for macromolecules. In *Computational chemistry* (Sayre, D., ed.), pp. 303-317. Clarendon Press, Oxford.
53. Brünger, A. T., Adams, P. D., Clore, G. M., DeLano, W. L., Gros, P., Grosse-Kunstleve, R. W., Jiang, J. S., Kuszewski, J., Nilges, M., Pannu, N. S., Read, R. J., Rice, L. M., Simonson, T. & Warren, G. L. (1998). Crystallography & NMR system: A new software suite for macromolecular structure determination. *Acta Crystallogr.* **D54**, 905-921.

54. Winn, M. D., Isupov, M. N. & Murshudov, G. N. (2001). Use of TLS parameters to model anisotropic displacements in macromolecular refinement. *Acta Crystallogr D Biol Crystallogr* **D57**, 122-33.
55. Kissinger, C. R., Gehlhaar, D. K. & Fogel, D. B. (1999). Rapid automated molecular replacement by evolutionary search. *Acta Cryst.* **D55**, 484-491.
56. Nicholls, A., Bharadwaj, R. & Honig, B. (1993). GRASP—graphical representation and analysis of surface properties. *Biophys J* **64**, A116.

ACCEPTED MANUSCRIPT

FIGURE LEGENDS

Figure 1. Strand discrimination by ED-10 Fab. (A) DNA sequences of the family of different length oligonucleotides. (site 35-18A, site 35-18B): 18-mer sequence corresponding to strand A and B of the HPV-16 site 35. (site 35-10B, site 35-6B, site 35-4B, site 35-3B, site 35-2B): 10-mer, 6-mer, 4-mer, 3-mer and 2-mer oligonucleotides containing the 5' end of site 35-18 B. (site35-48B): 48-mer B strand containing the site 35-18 sequence in the middle. (iset 35-48 B): Similar to site 35-48B, but with a random sequence instead of the site 35-18 sequence at the center of the oligonucleotide. (site 35-80 A): An 80-mer strand containing the site 35-18 sequence in the middle. (B) Strand discrimination by ED-10 Fab. Logarithmic plot of the binding of ED-10 Fab to site 35-18ds (closed diamonds), site 35-18 strand B (open circles) and site 35-18 strand A (closed triangles). The figure shows the titration of ED-10 Fab (5 nM) for 35-18ds and 35-18 strand B or ED-10 (50 nM) for 35-18 strand A. The changes in fluorescence of each isotherm were normalized against the major value. The binding data for ED-10 Fab to all the sequences tested are shown in Table I. (C) Electro Mobility Shift Assay (EMSA). Left panel 35-18ds; middle panel 35-18 Bss and 35-18 Ass; Right panel 35-80 Ass and 35-80 Bss.

Figure 2. Alpha carbon trace ED-10 and ED-10/DNA Fab fragments. (A) The two molecules (unbound and bound; left and right respectively) have been oriented in the same way that the light chain on the left (light gray) and the heavy chain on the right (darker gray). The DNA (ball-and-stick) appears with carbon, nitrogen, oxygen and phosphorus atoms colored in white, blue, red, and magenta, respectively and the CDRs are color coded as follows: L1, orange; L2, magenta; L3, green; H1, cyan; H2, pink; H3, yellow. (B) Stereo view of the electron density for the 5'dTdc3' contoured at 3.5σ .

Figure 3. ED-10 CDR H2 compared with the four canonical classes defined for H2 CDRs. The ED-10 is shown on the right (magenta) with side chains in a ball-and-stick representation. On the left, the ED-10 H2 (magenta) is superimposed with H2 CDRs from Hy-HEL10 (green, class I, no inserts after residue H52), Hy-HEL5 (yellow, class 2, 1 insert after residue H52), J539 (blue, class 3, 1 insert after residue H52), and 4-4-20 (cyan, class 4, 3 inserts after residue H52). The ED-10 H2 loop has a deletion of residue H54, and so is one residue shorter than the class I CDRs.

Figure 4. Stereo view of the ED-10/DNA combining site. Protein CDR loops, their side chains, and the DNA are colored as in Figure 2A. Hydrogen bonds between DNA and Fab are shown as black dotted lines.

Figure 5. Electrostatic surface representation of Fab ED-10. (A) ED-10 Fab. (A) ED-10 Fab/DNA complex. The CDR H3 residues H96-H98 are shown under the transparent surface to illustrate their rearrangement to form a cavity to allow DNA binding. The representation was produced using GRASP⁵⁶.

Figure 6. UV-circular dichroism analysis of free and bound ED-10. ED-10 was incubated at 5 μ M alone (dotted line) or complexed with equimolar concentrations of 35-4B (solid line). The spectrum of 5 μ M 35-4 B alone (dotted-dash line) and the sum of both spectra (dash line) are also presented. (A) far-UV CD spectra. (B) near-UV CD spectra.

Figure 7. Comparison of different D-ARM motifs. (A) The C2 binding site of ED-10; (B) the T2 binding site of DNA-1²⁵; (C) The mononucleotide binding site of Jel 103²² and (D) The T2 binding site of BV04-01²⁰. The CDR loops and their side chains are colored as in Fig. 2A.

Table 1. DNA Binding of Different Oligonucleotides to ED-10 mAb.

DNA	K_D^1 (nM)	ΔG^2 (kcal.mol ⁻¹)	$\Delta\Delta G^3$ (kcal.mol ⁻¹)
site 35-18ds	2.33 ± 0.4	-11.76	0
site 35-18 A	2319 ± 180	-7.68	5.14
site 35-18 B	0.39 ± 0.04	-12.82	0
iset 35-48ds	531 ± 80	-8.55	3.21
site 35-48ds	481 ± 28	-8.61	3.15
site 35-10 B	0.2 ± 0.02	-13.21	-0.40
site 35-6 B	0.27 ± 0.03	-13.04	-0.22
site 35-4 B	0.12 ± 0.01	-13.52	-0.70
site 35-3 B	0.18 ± 0.02	-13.28	-0.46
site 35-2 B	0.35 ± 0.03	-12.88	-0.06
dThymidine	2.8 ± 0.5	-11.65	1.17
site 35-18 B5'C	1600 ± 120	-7.90	4.92
site 35-18 B5'G	2113 ± 180	-7.73	5.09
site 35-18 B5'A	2487 ± 250	-7.64	5.18
site 35-80ds	1.71 ± 0.18	-11.95	-0.18
site 35-80A	0.15 ± 0.04	-13.39	-0.57
site 35-80B	610 ± 40	-8.47	4.35

¹ The stoichiometry is 1:1 for all sequences that were tested

² $\Delta G = -RT \ln K$

³ $\Delta\Delta G = \Delta G_T - \Delta G_{35-18ds}$ for double stranded DNA and $\Delta G_T - \Delta G_{35-18 B}$ for single stranded DNA

Table 2. Data collection and refinement statistics

	<i>Fab ED10</i>	<i>Fab ED10 + DNA</i>
Data collection		
Synchrotron, beamline	ESRF, ID14-1	LNL SB, D03B-MX1
Wavelength (Å)	0.9763	1.427
Resolution (Å) ¹	2.73 (2.8-2.73)	1.89 (1.92-1.89)
Space group, a,b,c (Å)	P2 ₁ 2 ₁ 2 ₁ ; 60.5, 86.8, 189.9	C2; 124.1, 64.2, 84.1, β=116.3°
No. of observations	96108 (9239)	110195 (5226)
No. of unique reflections	27701 (2699)	44585 (2106)
Completeness (%)	97.9 (97.0)	94.5 (91.5)
R _{sym} (%) ²	11.0 (45.3)	4.6 (43.3)
Average I/σ	16.0 (3.7)	17.2 (2.0)
Refinement statistics ³		
Resolution (Å)	2.73-25.40 (2.80-2.73)	1.89-40.50 (1.94-1.89)
No. reflections (working set)	26314 (1619)	42211 (2943)
No. reflections (test set)	1349 (84)	2235 (157)
R _{cryst} (%) ⁴	18.6 (34.6)	19.4 (32.5)
R _{free} (%) ⁵	26.2 (38.1)	22.8 (40.1)
No. of Fab atoms	6700	3350
No. of DNA atoms	0	35
No. of waters	0	180
Average B-values (Å ²)		
variable	34.6; 32.9	31.8
constant	28.2; 27.8	36.5
DNA	na ⁶	27.4
Wilson B-value (Å ²)	47.2	29.7
Ramachandran Plot		
Most favored (%)	86.3	89.6
Additionally allowed	12.5	9.9
Generously allowed	0.8	0.3
Disallowed	0.4	0.3
RMSD		
Bond lengths (Å)	0.024	0.019
Angles (Å)	2.14	1.86

¹Numbers in parentheses are for the highest resolution shell of data.

² $R_{\text{sym}} = \sum_{\text{hkl}} |I - \langle I \rangle| / \sum_{\text{hkl}} I$

³All reflections > 0.0σF

⁴ $R_{\text{cryst}} = \sum_{\text{hkl}} |F_o - F_c| / \sum_{\text{hkl}} |F_o|$

⁵R_{free} is the same as R_{cryst}, but for 5% of the data excluded from the refinement

⁶Not assessed**Table 3.** Hydrogen bonding and salt bridge distances between Fab ED-10 and water molecules to dTdC.

Fab or Water Atom	DNA Atom	Distance (Å)
His ^{L27d} NE2	Cyt ² O1P	2.71
Gly ^{L91} O	Cyt ² N4	2.69
Asn ^{H35} ND2	Thy ¹ O4	2.8
Gly ^{H98} N	Cyt ² O2	2.66
Wat ²⁸ O	Cyt ² O1P	2.54
Wat ¹⁶ O	Cyt ² O2	2.91
Wat ⁴ O	Cyt ² N3	2.81
Wat ⁸ O	Cyt ² N4	3.13

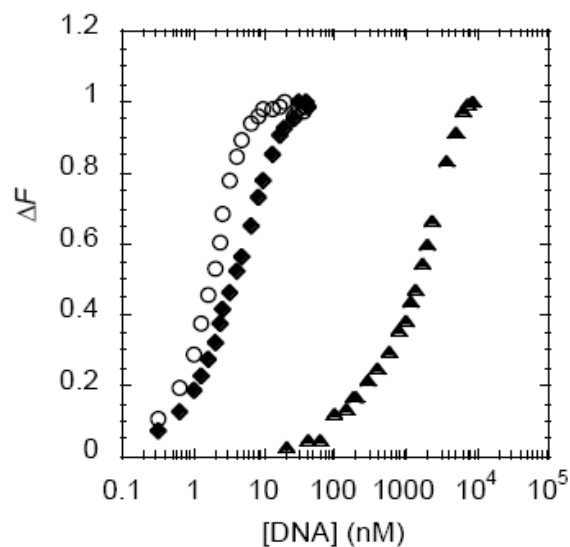
Hydrogen bonds evaluated with HBPLUS⁵⁷ and Contacsym⁵⁸

Figure 1.

(a)

site 35-18 A 5'-GTA ACC GAA ATC GGT TGA-3'
 site 35-18 B 5'-TCA ACC GAT TTC GGT TAC-3'
 site 35-10 B 5'-TCA ACC GAT T-3'
 site 35-6 B 5'-TCA ACC-3'
 site 35-4 B 5'-TCA A-3'
 site 35-3 B 5'-TCA-3'
 site 35-2 B 5'-TC-3'
 site 35-48 B 5'-TGT G(...)TCA ACC GAT TTC GGT TAC(...)G GGC-3'
 iset 35-48 B 5'-TGT G(...)TAC TTG ACA GGT CCA TGT(...)G GGC-3'
 site 35-80 A 5'-TCT T(...)GTA ACC GAA ATC GGT TGA(...)G ACG-3'

(b)



(c)

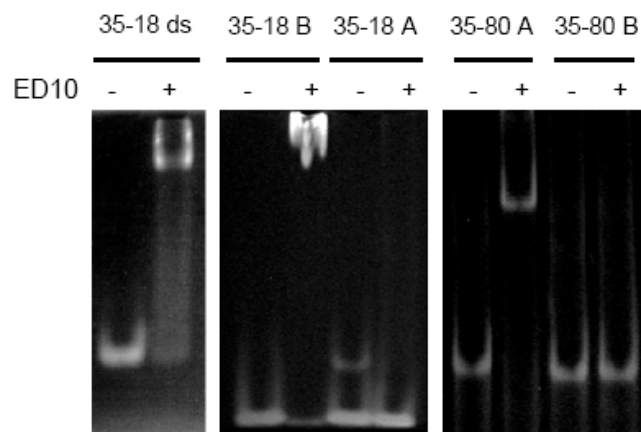


Figure 2.

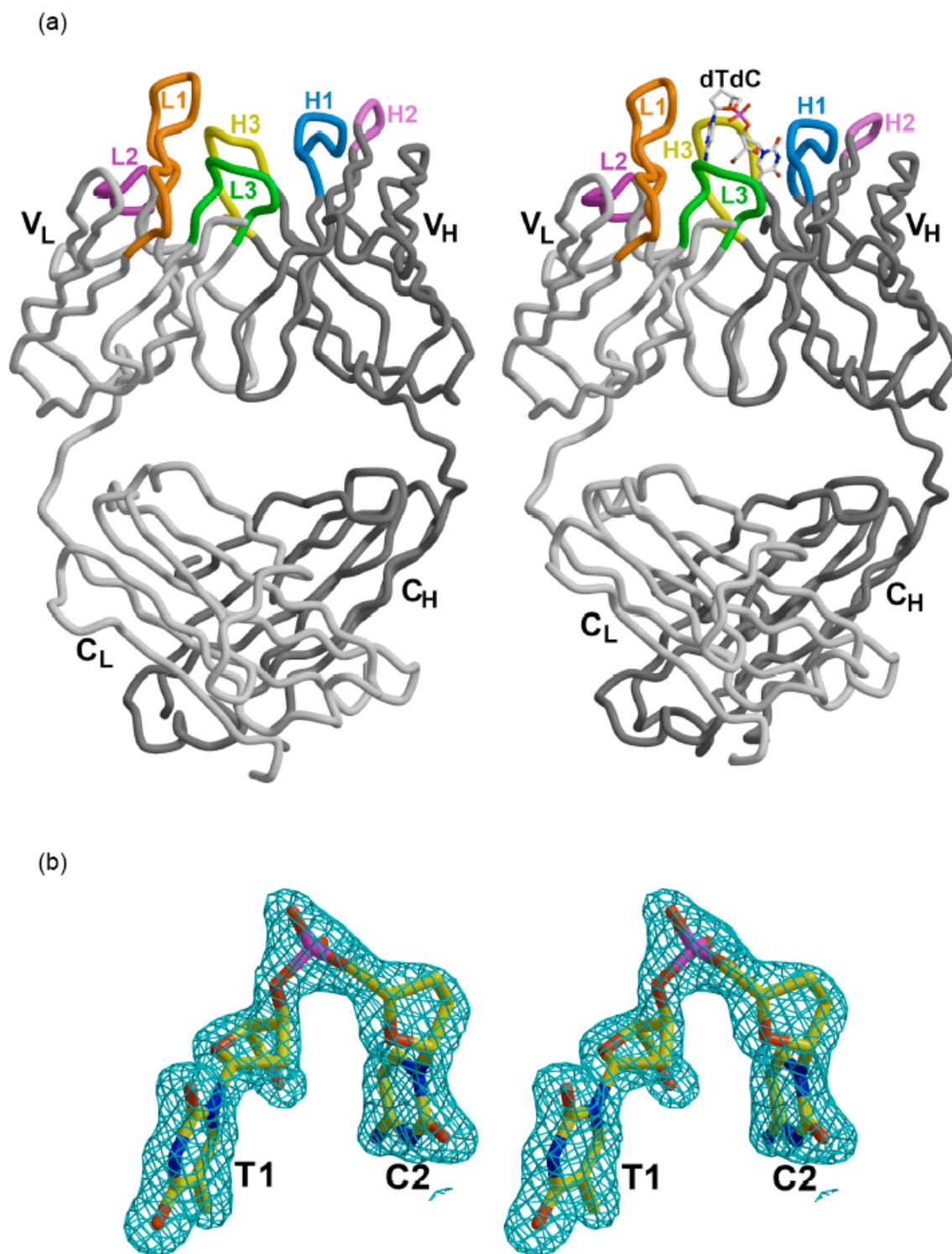


Figure 3.

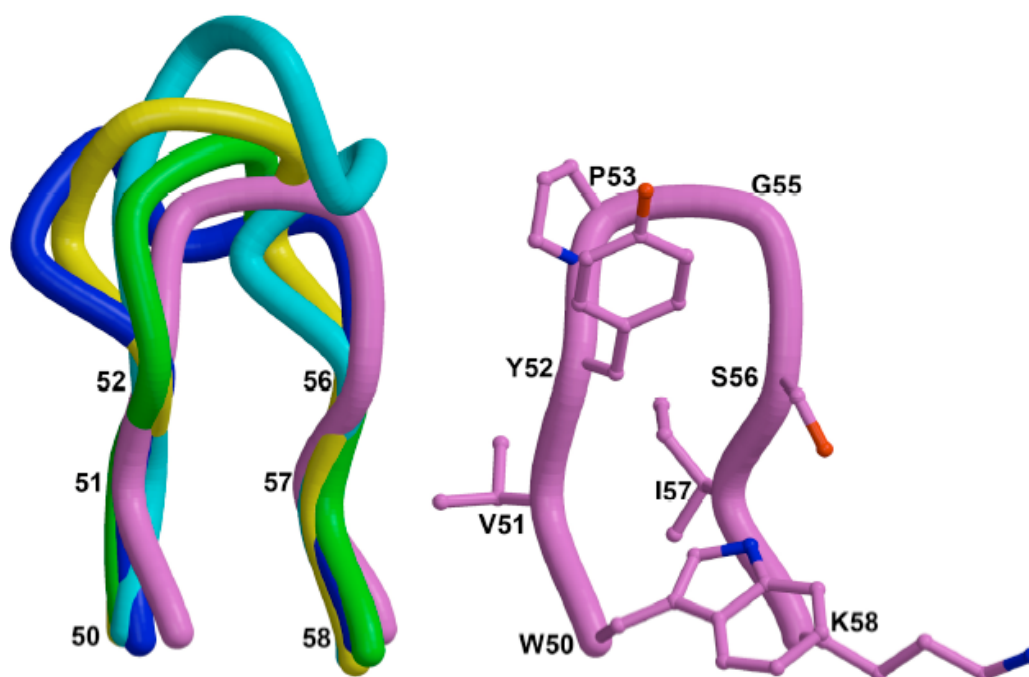
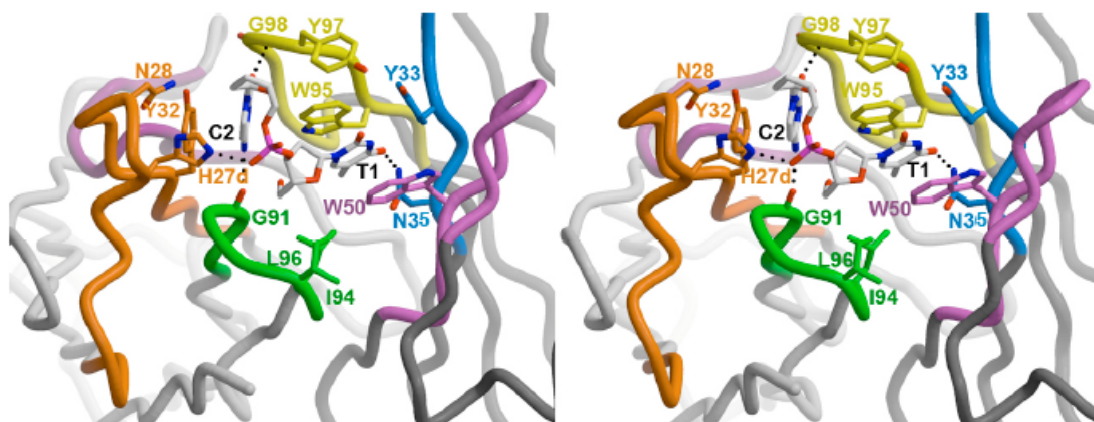


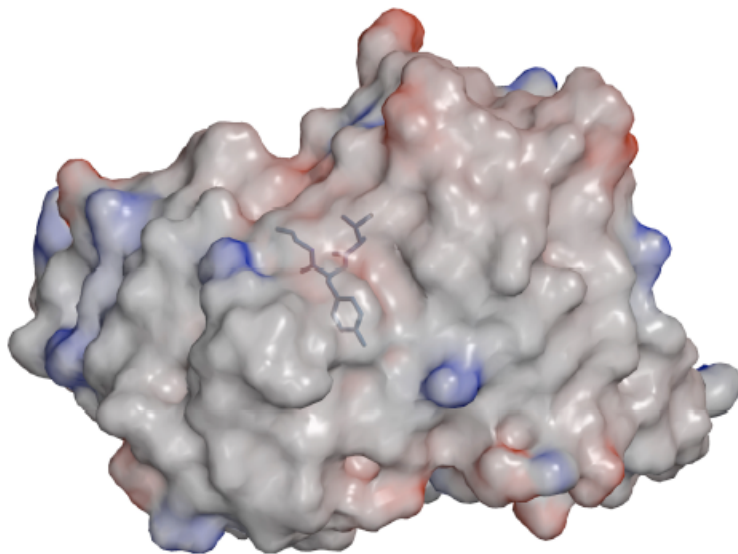
Figure 4.



ACC

Figure 5.

(a)



(b)

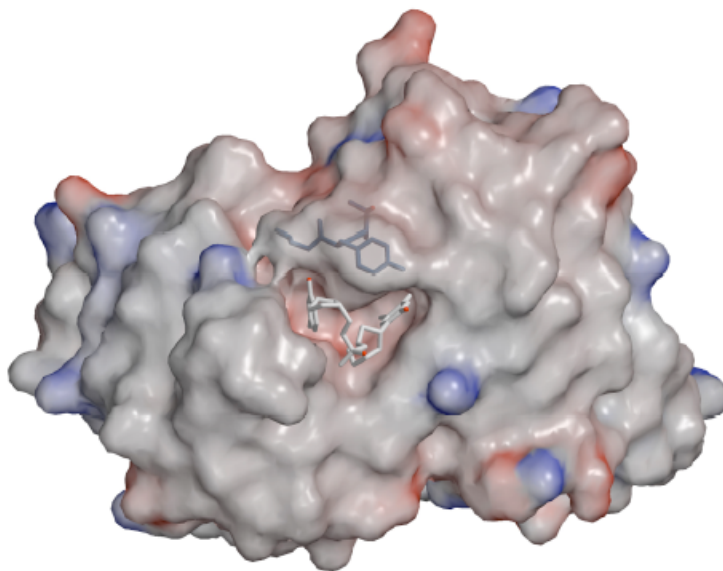
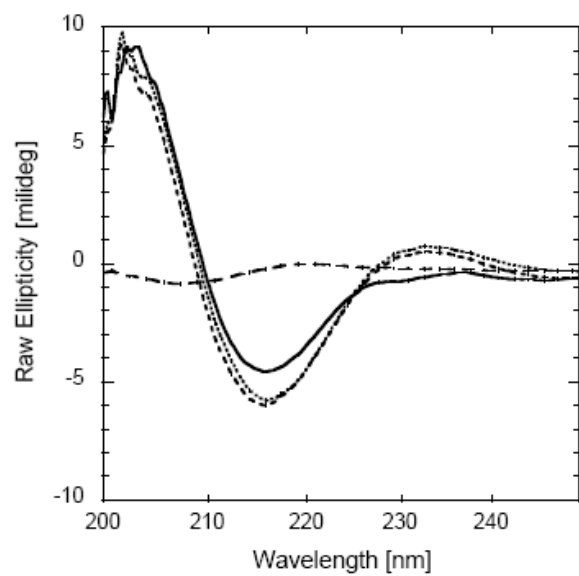


Figure 6.

(a)



(b)

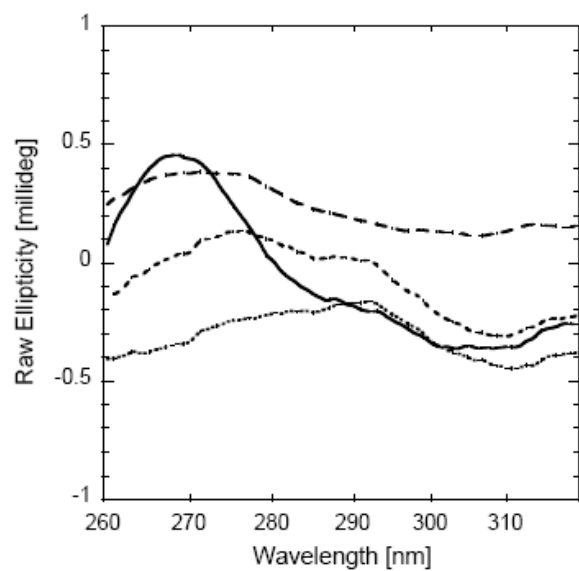


Figure 7.

